

# Substrate Coating Produced via Additive Manufacturing with Conducting Polymers: Assessment in The Development of Electrodes

José Victor B. D. Silveira<sup>a</sup>, Maurício F. de Aguiar<sup>a</sup>, Jardel J. O. Silva<sup>a</sup>, Celso P. de Melo<sup>b</sup>,  
César A. S. Andrade<sup>c</sup>, Alberto G. Silva-Junior<sup>c</sup>, Helinando P. de Oliveira<sup>d</sup> , Kleber G. B. Alves<sup>a\*</sup> 

<sup>a</sup>Universidade Federal de Pernambuco, Departamento de Engenharia Mecânica, 50670-901, Recife, PE, Brasil.

<sup>b</sup>Universidade Federal de Pernambuco, Departamento de Física, 50670-901, Recife, PE, Brasil.

<sup>c</sup>Universidade Federal de Pernambuco, Departamento de Bioquímica e Biofísica, 50670-420, Recife, PE, Brasil.

<sup>d</sup>Universidade Federal do Vale do São Francisco, Instituto de Pesquisa em Ciência dos Materiais, 48902-300, Juazeiro, BA, Brasil.

Received: December 06, 2022; Revised: May 17, 2023; Accepted: June 19, 2023

The production of conductive and organic devices from a 3D printer represents a promising strategy for several areas. In particular, the synthesis of polypyrrole-coated acrylonitrile butadiene styrene (ABS) composites can be considered an important step to produce conductive supports for 3D printing. Herein, it is reported the production of ABS samples through the additive manufacturing process (3D printing) accordingly to the Fused Deposition Modeling (FDM) method. The hydrophilic behavior was controlled by the surface treatment using air plasma for the following step of coating with polypyrrole (PPy) via an *in situ* polymerization, using two different oxidants: ferric chloride ( $\text{FeCl}_3 \cdot 6\text{H}_2\text{O}$ ) and ammonium persulfate (APS). The chemical, optical, surface, and electrical properties of these materials were characterized through Fourier Transform infrared spectroscopy (FTIR), contact angle measurements, cyclic voltammetry, Scanning Electron Microscopy (SEM), 4-probe electrical measurement, and mechanical tensile testing. The ABS/PPy ( $\text{FeCl}_3$ ) composite exhibited a low electrical contact resistance and better performance for applications that require electrodes with a good conductance level.

**Keywords:** Additive manufacturing, ABS, Conductive polymer, Polypyrrole.

## 1. Introduction

Additive manufacturing (AM) technology, first introduced in the 1980s for model building and prototyping, has been commercially available in various forms of 3D printers<sup>1</sup>. Unlike conventional conformity and subtractive manufacturing, the strength of 3D printing is the ability to manufacture high-quality, customizable parts from polymers, metals, and ceramics without the requirements from expensive molding or machining procedures<sup>1,2</sup> favoring the development of shorter and less expensive new product development cycles, through the additive manufacturing technique, it is possible to revalidate geometries and models. In addition to being widely applied in the area of product development and design, the technique is already well known in the medical field for making custom surgical guides and prostheses, for the acquisition of tomographic data and to produce a CAD file that can be a 3D printed template to reproduce the dimensions and specific features of each patient in a personalized way<sup>3,4</sup>. Furthermore, the use of several new materials, including nanomaterials, functional/smart materials, or even quick-drying concrete, has become possible, enabling

the technique to be applied in the civil construction and architecture market. 3D printing technology has already been shown to allow the manufacture of several houses in a single day<sup>5-7</sup>. In the electronics industry, the technique has been heavily used in the fabrication of devices capable of storing electrochemical energy, where the unique properties offered by 3D printing can be explored<sup>8</sup>. Some studies already report that carefully designed 3D structures show better performance in batteries and supercapacitors<sup>9,10</sup>. In addition, some studies have incorporated conductive polymers in the 3D printing process, enabling applications in gas sensing<sup>11,12</sup> and also in the field of biomedical applications for bone regeneration and drug transport throughout the body<sup>13-15</sup>.

All of these technological achievements show that 3D printing has the potential to revolutionize the traditional manufacturing process, from the aerospace industry to construction and electronics<sup>16</sup>. Conducting polymers represent a new class of electronic materials that have attracted growing interest in additive manufacturing, due to the competitive advantages of their electronic and optical properties over conventional polymers, with applications in artificial muscles, manufacturing of electronic devices, solar energy

\*e-mail: [kleber.gbvalves@ufpe.br](mailto:kleber.gbvalves@ufpe.br)

conversion, rechargeable batteries, and sensors<sup>17</sup>. Within this class of materials, one of the conductive polymers that stand out is polypyrrole (PPy), due to its easy synthesis, stability in oxidized form, high electrical conductance, and good redox properties<sup>18</sup>. These excellent intrinsic properties make PPy a potential candidate for several applications, such as supercapacitors, batteries, biosensors, antistatic coatings, textiles and fabrics, and shielding<sup>19</sup>. Furthermore, PPy has excellent stimuli-responsive properties that make it a very intelligent biomaterial, allowing the dynamic control of its properties by applying an electric field<sup>20</sup>. Herein, it is proposed a simple and efficient procedure to be applied in the chemical modification of ABS-based 3D printed surfaces with low resistance levels. With this aim, the general procedure for the polypyrrole deposition on ABS substrate was conducted to preserve good mechanical properties of the substrate incorporating outstanding properties of the conducting polymers. Two different oxidants (ferric chloride and ammonium persulfate), were explored as a part of a strategy to synthesize the composite samples, characterized through their chemical, optical, morphological, electrical, and mechanics through different techniques.

## 2. Experimental Section

### 2.1. Materials

The acrylonitrile-butadiene-styrene filament was obtained from 3D Fila, Brazil. The pyrrole monomer and the ammonium persulfate (APS) were obtained from Sigma-Aldrich, USA. The ferric chloride hexahydrate ( $\text{FeCl}_3 \cdot 6\text{H}_2\text{O}$ ) was obtained from Dinâmica, Brazil. The potassium hydroxide (KOH), the sulfuric acid ( $\text{H}_2\text{SO}_4$ ), and the potassium chloride (KCl) were obtained from Sigma-Aldrich, Brazil. The deionized water ( $\text{H}_2\text{O}$ ) used in all experiments was obtained from an ultrapure water purification system from Millipore, USA.

### 2.2. Synthesis of ABS samples

The samples were modeled via SolidWorks v2018 (Dassault Systèmes, Vélizy-Villacoublay, France) and the Simplify 3D software (v. 3.0.2) was used as the slicer to configure the G code for the two types of samples that were produced. The first type, a square sample of 15 mm x 15 mm of ABS (225 mm<sup>2</sup>) with a thickness of 1 mm, and the second type, produced in the specifications of test specimens for tensile testing following ASTM D638-14 Type V. The ABS samples were manufactured using an FDM 3D printer ANET A8 - 2017 (Shenzhen, China) with a filament of 1.75 mm diameter and an extruder with a 0.4 mm nozzle diameter. For the filling, the process was settled with a 100% infill, the direction of the layers was +45°/-45° at 230°C and 90°C for the extruder and the heated bed, respectively. At the end of the printing process, the removal of samples only took place after the heated table reached ambient temperature (25°C), to avoid warping defects.

### 2.3. Coating of polypyrrole on ABS samples

The ABS sample was exposed to an air plasma treatment for 5 min under a vacuum of 300 mTorr, to improve the hydrophilic character of its surface, using a PDC-002 Plasma

Cleaner (Harrick, USA)<sup>21</sup>. To carry out the *in situ* polymerization of the pyrrole monomers, the samples were immersed in a beaker with deionized water. Then, 0.48 mmol of pyrrole was added to a (48 mL) aqueous solution in a (250 mL) beaker and the solution was stirred for 30 minutes<sup>21</sup>. The ABS samples were introduced into the beaker, and the stirring was allowed to proceed for an additional period of 30 minutes. Finally, (2 mL) of a 0.24 M solution of ferric chloride was added to induce the polymerization, with a constant stirring being maintained for different amounts of time (2, 4, 6, 8, and 24 h). Afterward, the newly-formed ABS/PPy ( $\text{FeCl}_3$ ) samples were collected, washed several times with deionized water, and dried under ambient conditions. For samples that were coated with polypyrrole, using ammonium persulfate, the polymerization procedure followed the same steps, only adjusting the concentration of the prepared solution (2 mmol of pyrrole to prepare a 1 M solution of APS). The complete scheme of production of the preparation of electrodes for the following step of polymerization is shown in Figure 1 in which a single sample was coated per step.

### 2.4. Characterization

The wettability of the samples was evaluated using static water drops in a CAM 100 contact angle meter (KSV, Finland) using 15 samples per polymerization process ( $\text{FeCl}_3$  and APS). Contact angles were determined 30 s after the contact of the drop of 10  $\mu\text{L}$  of distilled water and the surface. The surface morphology analysis was performed from a MIRA3 scanning electron microscope (TESCAN, CZ) under two different magnifications (5000x and 50000x). The corresponding Fourier Transform Infrared (FTIR) spectra were obtained in the 4000-600  $\text{cm}^{-1}$  range using a Perkin Elmer model Spectrum 400 with NIR/MIR measuring range, using the Total Attenuated Reflectance (ATR) accessory. The tensile test was obtained using an MTS Exceed Universal Tensile Test Machine - Series 40 Electromechanical Universal Testing Systems, Model E42.503 (MTS, China). The tensile test procedures followed the American Society of Testing Material (ASTM) D638 - 14 and the specimen selected was Type V. The 3D printing of the samples according to the following specifications: orientation of alternating layers between +45° and -45°; layer height of 0.2 mm and all samples were fully filled. The deformation rate adopted was 1 mm/min. The electrical response of the ABS/PPy samples was determined by four-probe measurements using a 2400 SourceMeter multimeter (Keithley, USA) under a voltage range of -1 V to 1 V, in a linear sweep mode. The resistance was then determined through a linear fitting from the current-voltage curves. Cyclic Voltammetry measurements were obtained using a  $\mu\text{Autolab PGSTAT 128N}$  Potentiostat/Galvanostat (Ecochemie, Netherlands), interfaced with NOVA 1.8 software.

## 3. Results and Discussion

### 3.1. Contact angle measurements

For samples produced in pure ABS, the calculated contact angle was  $87.1^\circ \pm 2.0^\circ$ , as shown in Figure 2a, in agreement with the results for the contact angle 3D printed ABS reported in

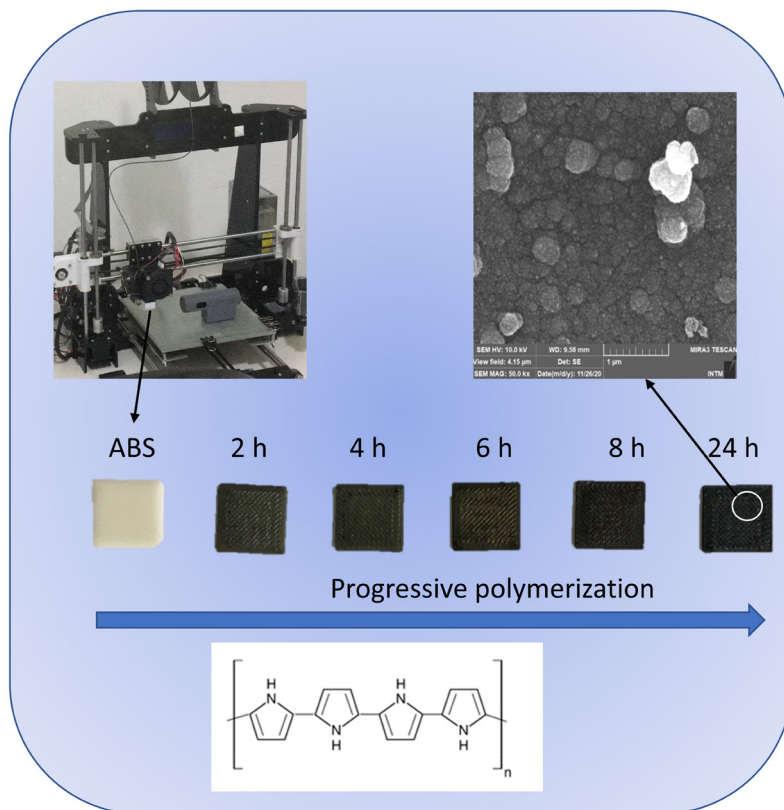


**Figure 1.** Schematic representation for the production of samples and the following polymerization at increasing time conditions.

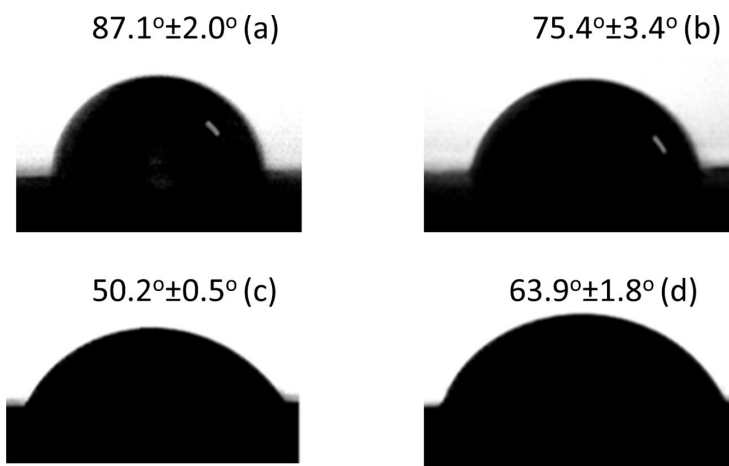


**Figure 2.** Contact angles of the ABS (a) and ABS-Plasma (b) and ABS/PPy(APS) (c) and ABS/PPy( $\text{FeCl}_3$ ) (d) samples.

the literature, which varies between  $81.0^\circ$  and  $99.5^\circ$ <sup>22,23</sup>. It was observed that after the application of the plasma, the contact angle of the pure ABS samples was reduced to approximately  $75.4^\circ \pm 3.4^\circ$ , as can be seen in Figure 2b. Literature reports the effect of the plasma treatment time in polymer samples used in 3D printing such as ABS, and indicated that the contact angle range can vary between  $95^\circ$  and  $41^\circ$  after plasma application for 30 min<sup>24</sup>. It was observed that, regardless of the oxidant used, after the coating with the conductive polymer, the general reduction in the contact angle value. As shown in Figure 2c, the values proved a greater reduction in the contact angle

for the case of samples coated with PPy (APS), for which the average contact angle was  $50.2^\circ \pm 0.5^\circ$ . For the samples coated with PPy ( $\text{FeCl}_3$ ), (Figure 2d), the mean value obtained was  $63.9^\circ \pm 1.8^\circ$ . Thus, the samples coated with polypyrrole showed a hydrophilic character, with the coating with PPy/APS leading to the most hydrophilic composite. It is known that the contact angle values for coating with polypyrrole can vary depending on the concentration of the oxidant used in the process<sup>25,26</sup>. The difference in wettability was also observed in other studies in the literature in which both oxidants were compared<sup>27,28</sup>. The differences observed in the contact angle

can be attributed to two different aspects: the first is the surface roughness due to the deposition of polypyrrole, in which a double structure is formed, and the second is the surface energy change due to the modification of the chemical composition of the polypyrrole<sup>27</sup>. The polypyrrole chains consist of a cation-charged conjugated backbone containing negatively charged counter-ions. This conductive polymer also has a wide range of wettability from hydrophobicity to hydrophilicity depending on the characteristics of the counterions and the doping level<sup>29-31</sup>.

### 3.2. Four-point probe resistance measurements

The conductance of the composite depends on the type and thickness of the PPy coating. From the four-point measurements (in which electrodes for current injection and voltage determination are independent – reducing effects of electrical contacts overall measurement of resistance), it was possible to obtain the electrical resistance values of the ABS samples coated with polypyrrole with two different oxidants (APS and  $\text{FeCl}_3$ ). The ABS/PPy ( $\text{FeCl}_3$ ) samples coated after 2 hours already presented a conductive character, with an average resistance of 2791.2  $\Omega$ . The ABS/PPy(APS) samples showed a higher resistance. For instance, the average resistance of the samples coated after 2 hours of pyrrole polymerization in the presence of APS was 25630.3  $\Omega$ , i.e., the samples prepared with APS exhibited a resistance 10 times higher than those of samples manufactured with  $\text{FeCl}_3$ . After 24 hours of PPy deposition, the average resistance value decreases to 2323.8  $\Omega$ . From the result shown in Figure 3, it is possible to notice the drop in the resistance value and the increasingly conductive behavior of the samples as a function of time. However, the coated parts that used the oxidizing ferric chloride, showed higher conductive levels throughout the experiment. For experiments in which the APS was used as an oxidant, the conductance was lower compared to that in  $\text{FeCl}_3$  due to the over-oxidation of the polymer conjugation main chain<sup>27,28</sup>.

### 3.3. Scanning electron microscope

The images of the pure ABS parts can be seen in Figures 4a and 4b. As can be seen, the surface is very irregular

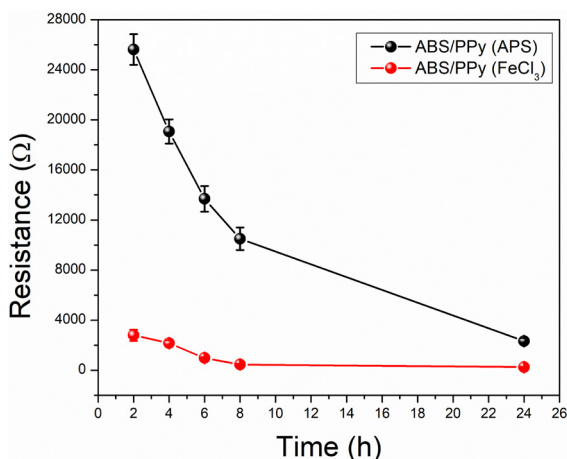


**Figure 3.** Electrical resistance as a function of the coating time in ABS/PPy samples.

with an accentuated roughness due to the non-uniform coating that takes place during the layer deposition process. The roughness and surface defects were also observed in some comparative studies between ABS parts printed in 3D by the FDM method and parts produced via plastic injection, in which the injected samples had a lower surface roughness and greater uniformity, while 3D printed samples had a more irregular surface<sup>32-34</sup>. Figures 4c and 4d show the SEM images of a cross-section of the ABS specimen before and after a tensile test, respectively. In Figure 4d, it is possible to identify the regions of voids due to the additive manufacturing process via the FDM method, the smaller dots, highlighted in the dotted region, are a natural characteristic of the process, as the cast filament is extruded in a cylindrical shape. As present in the literature, the dimension of the void regions in the 3D printed samples is directly associated with the height of the layer configured in the process and the diameter of the nozzle used, these void regions directly impact the mechanical properties of the parts produced via additive manufacturing<sup>35</sup>. It is also possible to identify two regions of a void that stand out due to a large discrepancy concerning the others, as indicated in the solid line region. In general, these defects are associated with discontinuity problems in the melt deposition flow; in turn, the flow discontinuity can be a slip failure between the tractor gear and the filament, or even a defect of bubbles in the material<sup>36</sup>. Figure 5a-d shows the results for the coating of ABS samples with polypyrrole using APS and  $\text{FeCl}_3$  as oxidants, respectively. As shown in the micrograph of the ABS/PPy (APS) samples, it was possible to cover the ABS surface with the conducting polymer layer. However, this coating occurred in a non-homogeneous way, as can be seen by the presence of some agglomeration points. The same happened with the ABS/PPy samples.  $\text{FeCl}_3$ . Another important point to highlight is the dependence of the coating based on time, as the surfaces of the coated samples after 24 hours of polymerization show a better homogeneity of distribution of nanoparticles when compared to the coated samples with times of 2, 4, 6, and 8 hours, both for the case of coating with either APS or  $\text{FeCl}_3$ . The oxidation-reduction potential of APS was higher than that of  $\text{FeCl}_3$ , causing a faster oxidation speed<sup>33</sup>. The fast oxidation speed increased the nucleation and growth rate of polypyrrole, resulting in the formation of metastable particles during the primary nucleation process. The metastable particles aggregated with each other through secondary nucleation to maintain a more stable state, thereby forming larger particles<sup>27,28</sup>.

### 3.4. Evaluation of the stress-strain of samples

The values obtained in the tensile test can be seen in Table 1 in which values for yield stress and strain rate for the ABS samples are in agreement with the results found in the literature<sup>37</sup>, whose results obtained for ABS with 100% filling (230 °C/100 °C), were 34.02 MPa for the yield stress and specific strain at break of 0.127 mm/mm, respectively. For tensile tests, the obtained average value for the yield stress limit was 4.0% lower in comparison with the value reported in the literature<sup>37</sup>. Such variation is due to the variability of ABS filament suppliers and the hotbed temperature, which for the test was 10°C lower. Other studies corroborate the

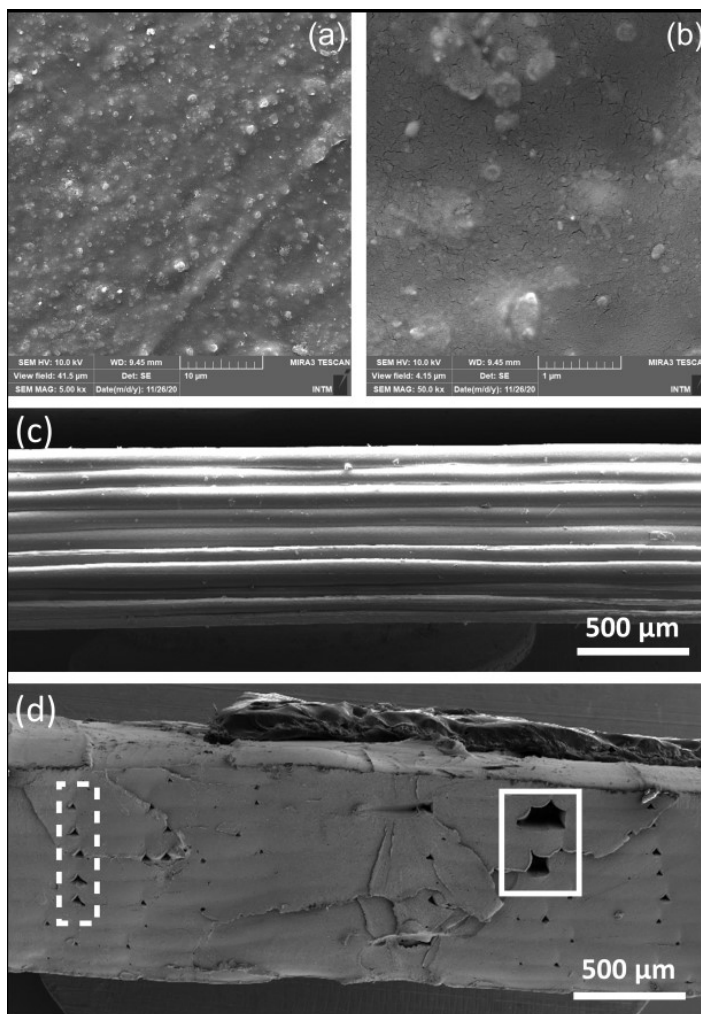


**Figure 4.** SEM micrograph of the ABS sample with different magnifications (a and b) and cross-section of the ABS specimen before (c) and after (d) a tensile test.

**Table 1.** Results of the tensile test of polypyrrole-coated ABS specimens.

Material	Yield Stress ( $\sigma_E$ ) [MPa]	Ultimate Tensile Strength ( $\sigma_R$ ) [MPa]	Young's Modulus ( $E$ ) [MPa]
ABS	$32.65 \pm 0.26$	$29.45 \pm 0.44$	$322.58 \pm 6.35$
ABS/PPy (APS)	$32.07 \pm 0.76$	$28.37 \pm 0.85$	$321.37 \pm 4.07$
ABS/PPy ( $FeCl_3$ )	$31.93 \pm 0.32$	$28.43 \pm 0.80$	$324.13 \pm 5.06$

results obtained for the yield stress limit, specific strain, and tensile strength limit<sup>38,39</sup>.

For the ABS/PPy (APS) specimens, the values found for the yield stress, rupture, and Young's modulus had very low variations in comparison with the values of the ABS specimens. For  $\sigma_E$ , there was a reduction of 1.8%. For  $\sigma_R$ , the reduction was 3.7% and for  $E$  the reduction was 0.4%. It is worth noting that the values obtained in the PPy-coated ABS test are within the range established by the standard deviation, thus, in a strong indication that the coating with conductive polymer did not affect the mechanical behavior

of pure ABS since it is a surface process of coating with minimal influence on bulky properties of the ABS substrate (no corrosive steps in the process).

### 3.5. Fourier transform infrared spectroscopy (FTIR)

The FTIR spectra of the ABS Samples (before and after the plasma treatment) and the hybrid ABS/PPy ( $FeCl_3$ ) and ABS/PPy (APS) are shown in Figure 6. The spectrum of ABS before plasma treatment is the same as the ABS sample after plasma treatment. The characteristic

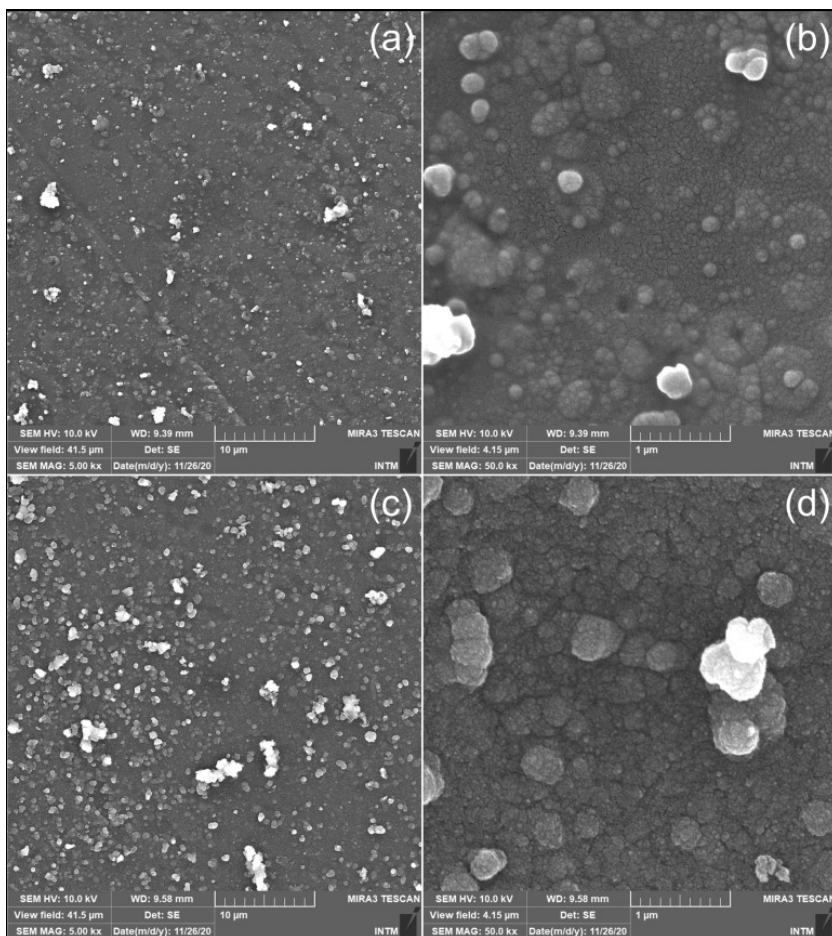


**Figure 5.** SEM micrograph of ABS/PPy (APS) substrates polymerized for 24 hours (a) – magnification of 5 kx, and b) magnification of 50 kx and ABS/PPy (FeCl<sub>3</sub>) substrates polymerized for 24 hours (c) magnification of 5 kx and d) magnification of 50 kx.

Acrylonitrile-butadiene-styrene bands, which are evident in Figures 6a and 6b, correspond to i) the C-H aromatic ring stretching at 3026 cm<sup>-1</sup>, ii) the C≡N axial stretching at 2237 cm<sup>-1</sup> characteristic of acrylonitrile group, iii) the C = N axial stretching and the C-C aromatic ring angular stretching at 1602 cm<sup>-1</sup>, iv) the C-H aromatic ring angular stretching and bending vibration at 1495 cm<sup>-1</sup>, v) the CH<sub>3</sub> asymmetric and symmetric stretching, respectively at 1453 and 1365 cm<sup>-1</sup>, vi) the C = C angular stretching at 966 cm<sup>-1</sup> and, finally, the vibration bands at 759 and 697 cm<sup>-1</sup> are related to C-H angular stretching of the monosubstituted aromatic ring and the out-of-plane angular stretching of the aromatic ring, respectively<sup>40-44</sup>. For the ABS samples treated with plasma, it was possible to identify the presence of all vibration bands characteristic of ABS, without highlighting extra peaks.

As could be expected, characteristic bands of both ABS and polypyrrole are present in the ABS/PPy spectrum. The characteristic PPy bands, which are evident in Figure 6c correspond to i) the pyrrole ring C=C and C-C stretching vibrations can be identified at 1559/1556 and 1473 cm<sup>-1</sup>, respectively<sup>45,46</sup>, ii) the pyrrole C-N stretching ring vibration at 1184 or 1185 cm<sup>-1</sup><sup>45,47,48</sup>, iii) the pyrrole C-H and N-H

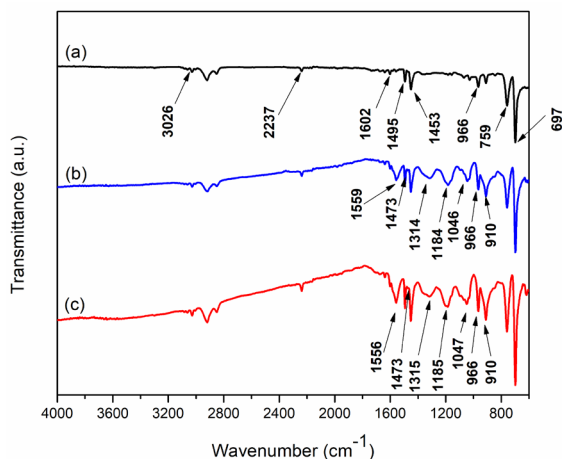


**Figure 6.** FTIR spectra of the ABS sample (a), ABS/PPy (FeCl<sub>3</sub>) (b), and ABS/PPy (APS) (c).

stretching vibrations can be identified at 1314/1315 and 1046 or 1047 cm<sup>-1</sup><sup>45,47,49</sup>, iv) the C-H out-of-plane angular stretching 965/966 and 910 cm<sup>-1</sup><sup>50,51</sup>.

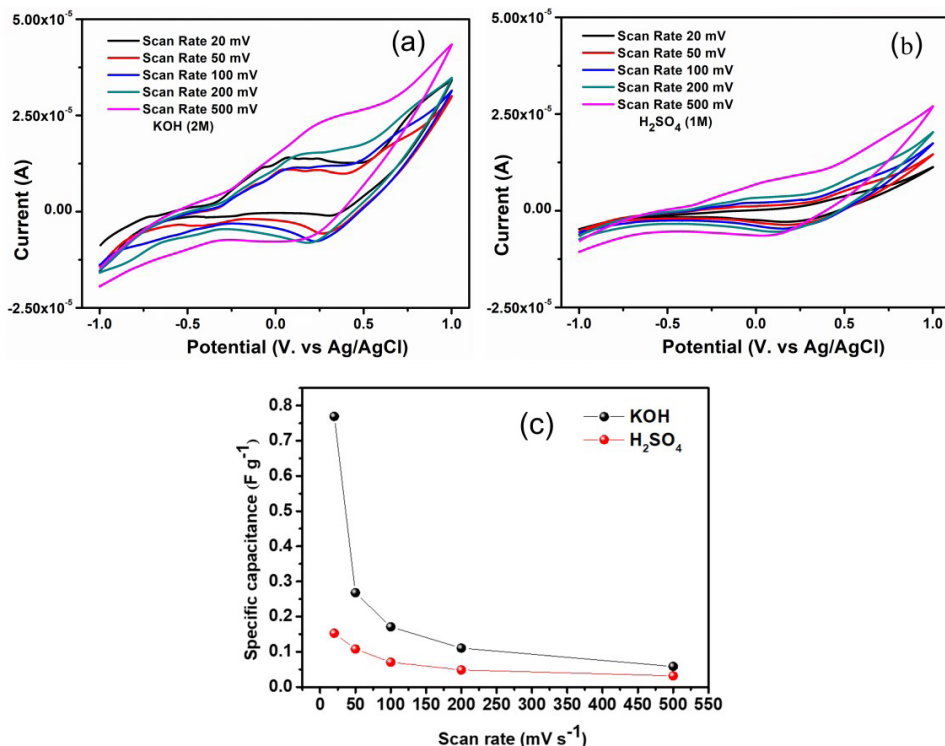


**Figure 7.** Cyclic voltammograms of ABS/PPy ( $\text{FeCl}_3$ ) with 24 hours of coating evaluated at different scan rates in KOH 2.0M (a) and  $\text{H}_2\text{SO}_4$  1M (b). The specific capacitance evolution as a function of scan rate is shown in (c).

### 3.6. Electrochemical measurements

The electrochemical properties of the ABS/PPy electrodes ( $\text{FeCl}_3$ ) with 24h of synthesis were determined through cyclic voltammetry performed at room temperature in the potential range of -1 V to +1 V (vs. Ag/AgCl) within the scan rates range of 20-500  $\text{mV s}^{-1}$  in 1 M  $\text{H}_2\text{SO}_4$  and 2M KOH. As expected for polypyrrole-based compounds, the shape migrates from a conventional rectangular shape of carbon derivatives to a prolate curve (cone-shaped behavior) as reported in the literature<sup>52</sup> (Figures 7a and 7b). The specific capacitance of the ABS/PPy electrodes was calculated from the obtained voltammograms, according to Equation 1:

$$C_{sp} = \frac{2A}{\Delta V \cdot \nu \cdot m} \quad (1)$$

where  $C_{sp}$  is the specific capacitance ( $\text{F g}^{-1}$ ),  $A$  corresponds to the integral area of the current-voltage curve,  $\Delta V$  is the potential window,  $\nu$  is the scan rate, and  $m$  is the weight of the material (in g).

As shown in Figure 7c, for both electrolytes, it was observed that the specific capacitance ( $\text{F g}^{-1}$ ) decreases with the increase in the scan rate, an expected result, due to the characteristic time of response for charge accumulation and redox reactions. As reported in the literature, this process is established at low scanning rates due to the appropriate time for the ions to diffuse into the pores and defects existing in the evaluated ABS/PPy ( $\text{FeCl}_3$ ), which plays an essential role in developing electric double layers<sup>53</sup>. Moreover, this result suggests that the composite is limited for redox transitions

at high scan rates based operation, leading to reduce electrochemical performance under increased scan rate<sup>54</sup>.

## 4. Conclusion

Through *in situ* polymerization, it was possible to effectively cover the ABS samples, produced via additive manufacturing. From the different times of exposure of the samples to the conducting polymer polypyrrole (PPy), the resulting material acquired good electrical performance for several applications. Concerning the influence of the oxidant on the overall response, the parts coated with ferric chloride ( $\text{FeCl}_3$ ) presented better electrical performance. The distribution of polypyrrole grains also proved to be more homogeneous for a longer coating process, as verified through the SEM analysis. From the contact angle test, it was possible to analyze the hydrophilic character of the regions coated with PPy for both oxidants, and it was also noted that the pieces that used APS as an oxidizer had a greater hydrophilic character. Regarding the mechanical properties of ABS parts (Yield Stress, Ultimate Tensile Strength, and Young's Modulus), they were not changed after coating with a conductive polymer, regardless of the oxidizer used. The maintenance of the mechanical properties of the parts is an important result of the study, as it represents a good compromise between the combination of electrical and mechanical properties. It was possible to confirm and reiterate the presence of polypyrrole in the coated samples through the FTIR test, the transmittance peaks detected for both oxidants were very close along the entire spectrum. Through

the cyclic voltammetry (CV) assays, it was possible to verify that the electrolyte immersed in KOH 2.0M presented the best electrical performance in terms of the peak electrical current in association with the maintenance of mechanical properties, given the two oxidants used. As a consequence, due to its lower electrical contact resistance, the ABS/PPy (FeCl<sub>3</sub>) composite proved to be more promising for the possible application that needs a good electrical response while maintaining the material's mechanical properties.

## 5. Acknowledgments

The authors acknowledge the financial support from the Brazilian institutions UFPE, CNPq and FACEPE (Grants APQ- 0916-3.03/14). This study was financed in part by the Coordenação de Aperfeiçoamento de Pessoal de Nível Superior - Brasil (CAPES) - Finance Code 001.

## 6. References

- Ngo TD, Kashani A, Imbalzano G, Nguyen KTQ, Hui D. Additive manufacturing (3D printing): a review of materials, methods, applications and challenges. *Compos. B. Eng.* 2018;143:172-96.
- Zhangwei C, Ziyong L, Junjie L, Chengbo L, Changyong L, Yang L, et al. 3D printing of ceramics: a review. *J. Eur. Ceram.* 2018;39:661-87.
- Sing SL, An J, Yeong WY, Wiria FE. Laser and electron-beam powder-bed additive manufacturing of metallic implants: a review on processes, materials and designs. *J Orthop Res.* 2016;34(3):369-85.
- Walker M, Humphries S. 3D Printing: applications in evolution and ecology. *Ecol Evol.* 2019;9:4289-301.
- Zhu C, Liu T, Qian F, Chen W, Chandrasekaran S, Yao B, et al. 3D printed functional nanomaterials for electrochemical energy storage. *Nano Today.* 2017;15:107-20.
- Wu P, Wang J, Wang X. A critical review of the use of 3-D printing in the construction industry. *Autom Construct.* 2016;68:21-31.
- Kira WS. China builds world's first 3D printed villa and tallest 3D printed apartment building [Internet]. 2015 (cited 2021 Mar 5). Available from: <https://3d-expo.ru/en/article/winsun-china-builds-world-s-first-3d-printed-villa-and-tallest-3d-printed-apartment-building>
- Lee CY, Taylor AC, Nattestad A, Beime S, Wallace GG. 3D printing for electrocatalytic applications. *Joule.* 2019;3(8):1835-49.
- Rolison DR, Long JW, Lytle JC, Fischer AE, Rhodes CP, Mcevoy TM, et al. Multifunctional 3D nanoarchitectures for energy storage and conversion. *Chem Soc Rev.* 2009;38:226-52.
- Osiak M, Geaney H, Armstrong E, O'dwyer C. Structuring materials for lithium-ion batteries: advancements in nanomaterial structure, composition, and defined assembly on cell performance. *J Mater Chem.* 2014;2:9433-60.
- Elwood J, Lin L. A 3D printed ethanol sensor using conformally-coated conductive polymer electrodes. In 20th International Conference on Solid-State Sensors, Actuators and Microsystems & Eurosensors XXXIII. Proceedings. New York: IEEE; 2019. p. 1230-3.
- Wu T, Gray E, Chen B. Self-healing, adaptive and conductive polymer composite ink for 3D printing of gas sensors. *J Mater Chem C Mater Opt Electron Devices.* 2018;6(23):6200-7.
- Zhou J, Vijayavenkataraman S. 3D-printable conductive materials for tissue engineering and biomedical applications. *Bioprinting.* 2021;24:e00166.
- Vijayavenkataraman S, Kannan S, Cao T, Fuh JYH, Sriram G, Lu WF. 3D-Printed PCL/PPy conductive scaffolds as three-dimensional porous Nerve Guide Conduits (NGCs) for peripheral nerve injury repair. *Front Bioeng Biotechnol.* 2019;7:266.
- Lawrence MT, Séguin C, Price A. 3D printed polypyrrole scaffolds for pH-dependent drug delivery for bone regeneration. In: Nano-, Bio-, Info-Tech Sensors and Wearable Systems. Proceedings. Washington: SPIE; 2021. p. 70-7.
- Shahrubudin N, Lee TC, Ramlan R. An overview on 3D printing technology: technological, materials, and applications. *Procedia Manuf.* 2019;35:1286-96.
- Ates M, Karazehir T, Sezai Sarac AJCPC. Conducting polymers and their applications. *Curr Phys Chem.* 2012;2(3):224-40.
- Benseddik E, Makhlonki M, Bernede JC, Lefrant S, Pron A. XPS studies of environmental stability of polypyrrole-poly(vinyl alcohol) composites. *Synth Met.* 1995;72(3):237-42.
- Panero S, Passerini S, Scrosati B. Conducting Polymers: new electrochromic materials for advanced optical devices. *Mol Cryst Liq.* 1993;229(1):97-109.
- Garner B, Georgevich A, Hodgson AJ, Liu L, Wallace CG. Polypyrrole-heparin composites as stimulus-responsive substrates for endothelial cell growth. *J Biomed Mater Res.* 1999;44(2):121-9.
- Aguiar MF, Leal ANR, Melo CP, Alves KGB. Polypyrrole-coated electrospun polystyrene films as humidity sensors. *Talanta.* 2021;234:122636.
- Yang H, Ji F, Li Z, Tao S. Preparation of hydrophobic surface on PLA and ABS by fused deposition modeling. *Polymers (Basel).* 2020;12(7):1539.
- Ji Y, Ma Y, Ma Y, Asenbauer J, Passerini S, Streb C. Water decontamination by polyoxometalate-functionalized 3D-printed hierarchical porous devices. *Chem Commun (Camb).* 2018;54(24):3018-21.
- Abourayana H, Dobbyn P, Dowling D. Enhancing the mechanical performance of additive manufactured polymer components using atmospheric plasma pre-treatments. *Plasma Process Polym.* 2017;15(3):1700141.
- Wang C, Wang Y, Song X, Huang M, Jiang H. A facile and general strategy to deposit polypyrrole on various substrates for efficient solar-driven evaporation. *Adv Susta Syst.* 2019;3(1):1800108.
- Yang X, Ma K, Yang L, Chen Y, Qu Y, Wang Y, et al. Influence of magnetic field on morphological structures and physiological characteristics of bEnd.3 cells cultured on polypyrrole substrates. *RSC Advances.* 2019;9(70):40887-94.
- Lee S, Park CH. Conductivity, superhydrophobicity and mechanical properties of cotton fabric treated with polypyrrole by in-situ polymerization using the binary oxidants ammonium Peroxodisulfate and ferric chloride. *Text Res J.* 2019;89(12):2376-94.
- Yussuf A, Al-Saleh M, Al-Enezi S, Abraham G. Synthesis and characterization of conductive polypyrrole: the influence of the oxidants and monomer on the electrical, thermal, and morphological properties. *Int J Polym Sci.* 2018;2018:1800108.
- Darmanin T, Guittard F. Wettability of conducting polymer: from superhydrophilicity to superoleophobicity. *Prog Polym Sci.* 2014;39:656-82.
- Xu L, Chen W, Mulchandani A, Yan Y. Reversible conversion of conducting polymer films from superhydrophobic to superhydrophilic. *Angew Chem Int Ed Engl.* 2005;44:6009-12.
- Lee S, Park CH. Conductivity, superhydrophobicity and mechanical properties of cotton fabric treated with polypyrrole by in-situ polymerization using the binary oxidants ammonium Peroxodisulfate and ferric chloride. *Text Res J.* 2019;89(12):2376-94.
- Paganin LC, Barbosa GF. A comparative experimental study of additive manufacturing feasibility faced to injection molding process for polymeric parts. *Int J Adv Manuf Technol.* 2020;109(9-12):2663-77.
- Xiaoran L, Guo J, Li W, Zhang L, Wang C, Guo B, et al. Analysis of morphology and electrical insulation of 3D printing parts.

- In International Conference on High Voltage Engineering and Application; Athens, Greece. Proceedings. New York: IEEE; 2018.
34. Vidakis N, Petousis M, Maniadi A, Koudoumas E, Kenanakis G, Romanitan C, et al. The mechanical and physical properties of 3D-printed materials composed of ABS-ZnO nanocomposites and ABS-ZnO microcomposites. *Micromachines (Basel)*. 2020;11(6):615.
  35. Garzon-Hernandez S, Garcia-Gonzalez D, Jérusalem A, Arias A. Design of FDM 3D printed polymers: an experimental-modelling methodology for the prediction of mechanical properties. *Mater Des*. 2020;188:108414.
  36. Tronvoll SA, Welo T, Elverum CW. The effects of voids on structural properties of fused deposition modelled parts: a probabilistic approach. *Int J Adv Manuf Technol*. 2018;97(9-12):3607-18.
  37. Žur P, Žur A, Baier A, Kokot G. Optimization of Abs 3D-printing method and parameters. *Eur J Eng Sci Tech (Paris)*. 2020;3(1):44-51.
  38. Rodríguez JF, Thomas JP, Renaud JE. Mechanical behavior of acrylonitrile butadiene styrene fused deposition materials modeling. *Rapid Prototyping J*. 2003;9(4):219-30.
  39. Alvarez K, Lagos R, Aizpun M. Investigating the influence of infill percentage on the mechanical properties of fused deposition modelled ABS parts. *Ing Invest*. 2016;36:110-6.
  40. Ferreira AC, Diniz MF, Mattos EC. FT-IR methodology (transmission and UATR) to quantify automotive systems. *Polímeros*. 2018;28(1):6-14.
  41. Smith AL. *Applied infrared spectroscopy*. New York: John Wiley & Sons; 1979.
  42. Zhang SU. Degradation classification of 3D printing thermoplastics using fourier transform infrared spectroscopy and artificial neural networks. *Appl Sciences*. 2018;8:1224.
  43. Liu G, Liao Y, Ma X. Thermal behavior of vehicle plastic blends contained acrylonitrile-butadiene-styrene (ABS) in pyrolysis using TG-FTIR. *J Waste Manag*. 2017;61:315-26.
  44. Truc N, Lee BK. Selective separation of ABS/PC containing BFRs from ABSs mixture of WEEE by developing hydrophilicity with ZnO coating under microwave treatment. *J Hazard Mater*. 2017;329:84-91.
  45. Fu Y, Manthiram A. Sulfur-polypyrrole composite cathodes for lithium-sulfur batteries. *RSC Advances*. 2012;2:5927-9.
  46. Tabačiarová J, Mičušík M, Fedorko P, Omastová M. Study of polypyrrole aging by XPS, FTIR and conductivity measurements. *Polym. Degrad*. 2015;120:392-401.
  47. Minisy IM, Bober P, Acharya U, Trchová M, Hromádková J, Pflieger J, et al. Cationic dyes as morphology-guiding agents for one-dimensional polypyrrole with improved conductivity. *Polymer (Guildf)*. 2019;174:11-7.
  48. Reung-U-Rai A, Prom-Jun A, Ouajai W, Ouajai S. Synthesis of highly conductive polypyrrole nanoparticles via microemulsion polymerization. *J Met Mater Miner*. 2008;18(2):27-31.
  49. Číková E, Mičušík M, Šišková A, Procházka M, Fedorko P, Omastová M. Conducting electrospun polycaprolactone/polypyrrole fibers. *Synth Met*. 2018;235:80-8.
  50. Alves KGB, Andrade CAS, Campello SL, Souza RE, Melo CP. Magnetite/polypyrrole hybrid nanocomposites as a promising magnetic resonance imaging contrast material. *J Appl Polym Sci*. 2013;128(5):3170-6.
  51. Sunilkumar A, Manjunatha S, Chethan B, Ravikiran Y, Machappa T. Polypyrrole-Tantalum disulfide composite: an efficient material for fabrication of room temperature operable humidity sensor. *Sens Actuators A Phys*. 2019;298:111593.
  52. Alcaraz-Espinoza JJ, Oliveira HP. Flexible supercapacitors based on a ternary composite of polyaniline/polypyrrole/graphite on gold coated sandpaper. *Electrochim Acta*. 2018;274:200-7.
  53. Konikkara N, Kennedy LJ. Electrochemical properties of solid leather wastes based supercapacitor electrodes using H2SO4 electrolyte. *Mater Lett*. 2017;205:56-61.
  54. Shinde SS, Gund GS, Kumbhar VS, Patil BH, Lokhande CD. Novel chemical synthesis of polypyrrole thin film electrodes for supercapacitor application. *Eur Polym J*. 2013;49(11):3734-9.